ELSEVIER

Global and Planetary Change 9 (1994) 29–38

GLOBAL AND PLANETARY CHANGE

A comparison of energy balance calculations, measured ablation and meltwater runoff near Søndre Strømfjord, West Greenland

R.S.W. van de Wal [a], A.J. Russell [b]

[a] *Institute for Marine and Atmospheric Research, Utrecht University, Princetonplein 5, 3584 CC Utrecht, The Netherlands*
[b] *Kingston University, School of Geography, Penrhyn, Kingston upon Thames, Surrey KT1 2EE, UK*

(Received June 9, 1992; revised and accepted December 29, 1992)

Abstract

This paper presents a comparison of measured ablation and calculated ablation based on an energy balance approach. The meteorological measurements for this study were conducted on the ice sheet in the Søndre Strømfjord area, West Greenland, during the 1990 and 1991 melt seasons as a part of the Greenland Ice Margin Experiment (GIMEX). The calculated ablation was used to force a model to predict proglacial meltwater runoff in the same area. Results are presented from a comparison between calculated and measured ablation as well as a comparison between measured and modelled discharge.

1. Introduction

To study the ablation of a glacierized region one can measure the ablation directly with stake readings during an ablation season. This reveals information on the ablation at a specific point. For extrapolation of this information to larger areas one needs to have a good insight in the physical processes. Energy balance calculations based on meteorological measurements provide such an insight. This paper compares the measured ablation with the calculated ablation using a simple energy balance model. Furthermore, calculated ablation will be compared with proglacial meltwater runoff measurements providing the cumulative ablation over a small sector of the Greenland Ice Sheet. This approach provides a better understanding of meltwater runoff processes as well as forming a base for the energy balance calculation for the whole Greenland Ice Sheet, which is the ultimate goal.

To achieve the comparison between measured ablation and measured meltwater runoff two steps have to be taken. Firstly, half hourly values of the ablation were calculated with an energy balance model. Energy balance calculations include shortwave and longwave radiation fluxes and the sensible heat flux and the latent heat flux, no englacial energy storage was taken into account. Calculation of the fluxes was based on measurements carried out during the GIMEX expeditions of 1990 and 1991. Secondly, calculated meltwater production needs to be converted to a runoff record. Calculated meltwater has to be transported from the ice sheet surface into proglacial rivers. To describe the routing of this water we used a simple runoff model, often applied in hydrology to describe river flow. This model is a modified version of the linear box model described by Baker et al. (1982), including a second order relation between the discharge and the volume of water stored in the boxes of the model.

SSDI 0921-8181(94)E0061-3

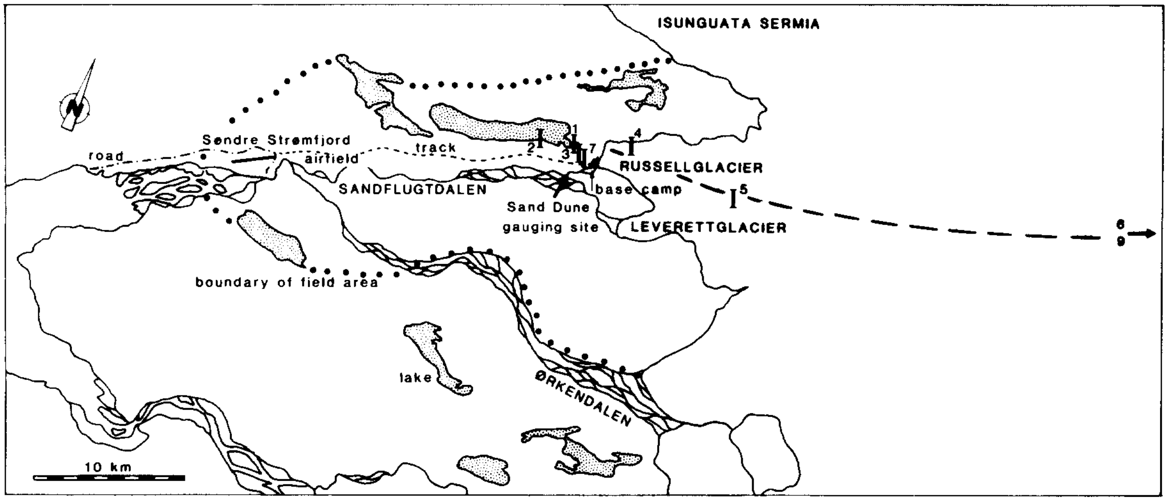

Fig. 1. A map of the study area. The ice sheet is at the right. The dashed line shows the mass balance transect (see Fig. 2 for location and elevation of stakes). The meteorological data used in this study come from site 4 on Russell Glacier.

This predicted meltwater runoff can then be compared with the measured meltwater runoff.

The study area consisting of a sector of the Greenland Ice Sheet immediately to the north east of Søndre Strømfjord (67°N 50°W) is characterised by relatively high ablation and low accumulation, with the annual accumulation amounting to roughly 100–150 mm water equivalents (we) (Ohmura and Reeh, 1991) and an annual mean temperature of −5°C. This site was chosen mainly for logistical reasons, with easy access, only 25 km from Søndre Strømfjord airport along a jeep track. Additionally the area is of particular interest as the equilibrium line altitude is judged to be one of the highest in Greenland giving a large ablation zone along the ice margin. Low accumulation rates lead to a relatively long period of bare ice exposure simplifying modelling of the ablation process.

During these two expeditions meteorological measurements were conducted both at three locations on the tundra and three on the ice. We will concentrate solely on the measurements close to the ice margin at mast 4 (Fig. 1). Meteorological measurements at the other sites are discussed in the papers by Van den Broeke et al. (1994) and Duynkerke et al. (1994). Stake readings were obtained from a profile extending from the ice

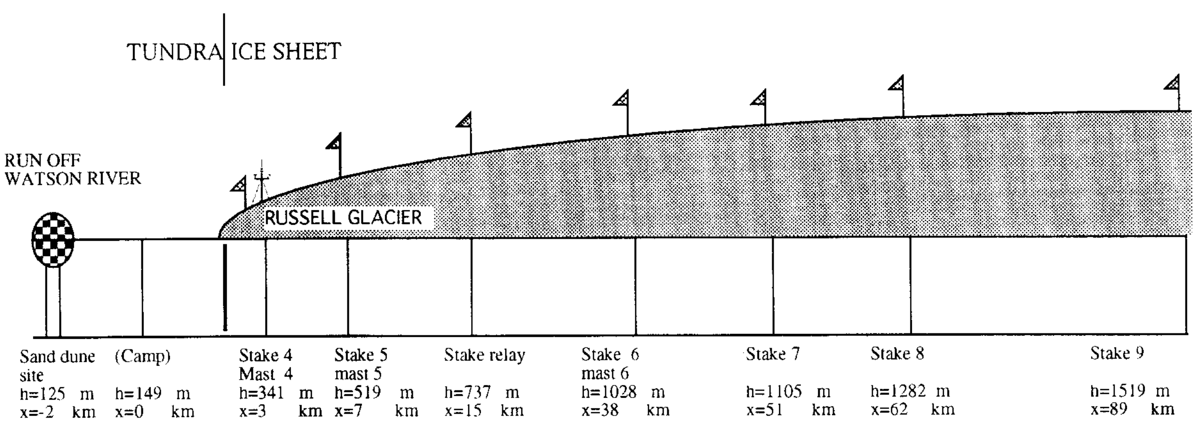

Fig. 2. The stake transect.

margin up to 1500 masl (Fig. 2). The discharge measurements were carried out in the Watson river at the Sand Dune Site (Fig. 1).

2. Measurements and data acquisition

2.1. Meteorological measurements

Here a description of the meteorological equipment is restricted to mast 4 which provides the main source of data used. Mast 4 is 6 m high with instruments at five levels. The range and precision of the applied sensors is presented in Table 1. Measurements were carried out during a period of 52 days starting June 10 and ending July 31, 1991. The mast has its own power unit, for ventilation of the temperature sensors and a local built-in computer. The power unit consists of a solar panel in combination with a regular 12V battery, and a lithium battery to overcome periods with extremely low insolation. The registration used was telemetric, RIDAS (radio interfacing data acquisition). A sampling frequency of 2 minutes was maintained for all the sensors during the entire period. In addition to the meteorological sensors, time, date, voltage of the battery, loading current of the solar panels and a dummy reference sensor were sampled. First data were stored locally at the mast. After some time the data were sent in packets of 70 minutes to the receiving computer in the base camp (Fig. 1).

In practice, a disturbance in the radio connection during up to 28 hours can be handled with this system without loosing data. Reduction of the sample interval to 10 minutes gives therefore 5×28 hours local storage memory. The sequential accumulation of data from all the stations is done in a fully computer-steered procedure. Online graphical display of the data enabled quick adjustments of the data acquisition procedure as well as a good physical insight in the on-going processes. In the morning the data of the previous day were reduced to 10 minutes, 30 minutes and hourly mean values, and simple energy balance calculations were performed. As calibration of the instruments has been done in advance, a complete "cleaned" and reduced data set was available a few hours after the last measurements. For this work we used specially developed data loggers, a standard radio receiver Kenwood TM 431A/TM 45, and a radio-telemetry system with packet radio using a baud rate of 1200 bits/s, at a frequency of 451 MHz. Transmission of the data takes approximately 4 hours for a whole day of measurements at 7 locations.

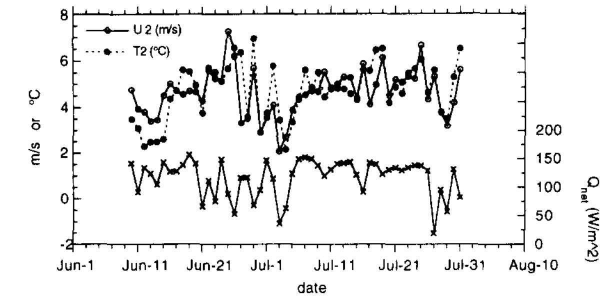

Fig. 3. Daily net shortwave radiation, temperature and wind speed at 2 m as a function of time for the 1991 field season at mast 4.

Table 1
Specification of the sensors and set up of mast 4

Sensor	Type	Range	Precision	Height (m)
Air temperature	Rotronic YA-100	−20–+28°C	0.05°C	0.5,2,6
Humidity	Rotronic YA-100	0–100%	2%	0.5,2,6
Wind speed	Aanderaa 2740	0.2–60 m/s	0.2 m/s	0.5,1,2,6
Wind direction	Aanderaa 2750	0–360∞	4∞	6
Sensor	**Type**	**Spectral range**	**Precision**	**Height (m)**
Pyranometer	Kipp CM14	305–2800 nm	2 W/m^2	1.5
Pyrradiometer	Aanderaa 2811	300–60000 nm	3 W/m^2	1.5

Fig. 3 summarizes the meteorological observations based on data of mast 4. Daily mean values of the temperature and wind speed and the net radiation are plotted as a function of time. Due to the dominating katabatic wind regime the temperature and wind speed are highly correlated, even the daily mean values. Clear sky conditions characterise the radiation in the studied period, only short periods of cold and rainy weather occurred on July 3,4 and 27.

2.2. Ablation measurements

In late summer 1989 a stake net was drilled consisting of 2 or 3 stakes at each of four locations (sites, 4, 5, relay, and 6, see Fig. 1 and 2). Unfortunately most of the stakes were never found again. Only the stakes close to the ice margin could be traced. Accurate positioning of the stakes with G.P.S. (Global Positioning System by Satellite) in 1990 added much to the recovery rate the following summer. The ablation measurements were performed with a long rod laid flat on the surface, as a reference level which was always orientated N–S. The measurements from the different stakes at one location were averaged to reduce local irregularities in ablation. Since only periods of at least 5 days were considered no significant anomalies were found between the stakes at any one location. The accuracy of this approach is estimated to be at least 5 cm. These measurements generated a yearly ablation profile with altitude as presented in Fig. 4. The linear fit shows an ablation gradient of 2.7 mm we/m comparable with other measurements in West Greenland [Thomsen (1987), Pakitsoq area (69°N); Braithwaite (1983), Qamanârssûp Sermia (64.5°N); Weidick (1984), a summary on West Greenland], which range from 2 to 4.5 mm we/m. The profile indicates an equilibrium line altitude (ELA) of 1700 m.a.s.l., which is 200 m higher than the estimate for the long term mean ELA as given by Weidick (1984). The good linear fit indicates that the point measurements do have a regional meaning and are not affected too much by local anomalies. Ablation measurements at mast 4 taken at one-week intervals will be discussed later when the energy balance calculations are presented.

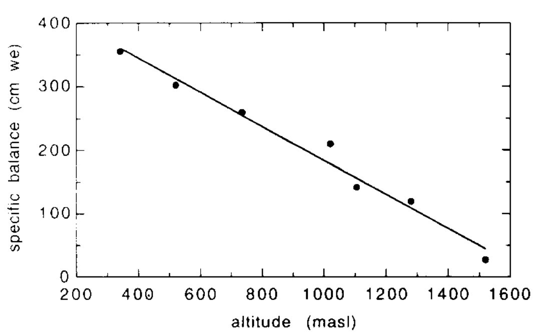

Fig. 4. The 1990/91 specific balance as a function of the altitude for the Søndre Strømfjord transect.

2.3. Discharge measurements

River discharge (Q_{meas}) was gauged 2 km downstream of the ice margin at the "Sand Dune" site from June 22 to July 31, 1991. River stage was recorded using a pressure transducer and data logger system averaging readings over 10 minutes. The river stage data were downloaded every week using a Macintosh portable computer. To determine river discharge, 20 river depth and velocity profiles were carried out for a representative range of stages during the entire gauging period. Velocities were measured with an Ott flow meter averaging over three readings, taken at 0.6 the depth every 2 m. River discharge for each profile was calculated using the velocity-area method (Herschy 1978), with an estimated accuracy of 10%.

The plot of stage against discharge shows a clear relationship from which a linear best fit equation was derived (figure 5). The assumption of a linear stage-discharge relationship appears reasonable considering possible changes in channel cross-sectional area over time and hysteresis effects. The entire discharge record for June 22–July 31 is presented later (Fig. 5).

2.4. Calculating the meltwater production

The energy available for melting (B) is a function of the radiative flux and the turbulent heat flux:

$$B = G(1-\alpha) + L_n + H + LE \quad (1)$$

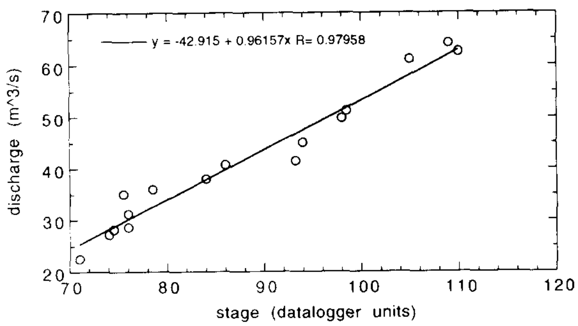

Fig. 5. The stage-discharge relation for the Sand Dune gauging site.

Where α is the surface albedo, G the global radiation (W/m^2), L_n the net longwave radiation (W/m^2), H the sensible heat flux (W/m^2) and, LE the latent heat flux (W/m^2). Fluxes towards the surface will be called positive and those from the surface negative, by definition. B can be converted to water equivalents using the latent heat of ice (3.34 10^5 J/kg). In this approach it is assumed that the temperature of the surface of the glacier is continuously at 0°C. For this particular area and period this is a reasonable assumption because the ambient temperature is always above zero even during the night. Nevertheless freezing of the surface occasionally occurs on the ice due to radiative cooling during the night. Although this effect is of minor importance, it is accounted for by compensation of the integrated negative energy loss during some nights in the morning, before allowing melt. The difference between this method and the simple summation of all positive energy fluxes is 8 mmwe on a total of 2.3 mwe.

The first term in Eq. (1) was obtained immediately from the measurements of incoming and reflected shortwave radiation. The second term was obtained by subtracting the measured shortwave radiation from the measured total radiation. Errors arising from this approach were difficult to estimate but might have been considerable. Nevertheless, it is assumed that the errors will be random, and therefore zero as a mean as long as the longwave radiation is considered over a whole day.

The physics of the turbulent fluxes are complicated, especially in a stable atmosphere as present above a melting ice surface. Although detailed flux measurements are needed to validate a simple bulk gradient relationship, we adopted the following equation:

$$H = \frac{\rho c_p k^2 (u_2)(T_2)}{\ln\left(\frac{z+z_0}{z_0}\right)\ln\left(\frac{z+r_0}{r_0}\right)} \tag{2}$$

where ρ is the density of the air, c_p the specific heat capacity, k the Von Karmann constant, u_2 the wind velocity at 2 m height (z), T_2 the temperature at 2 m height, and z_0 and r_0 the roughness length scale for momentum and heat. Measurements of the wind speed at heights of 6, 2, 1 m during the GIMEX expeditions indicate a roughness length scale for momentum of roughly 10^{-3} m which is in agreement with measurements by Hogg et al. (1982). All the constants can be reduced to one exchange coeficient for which we adopt a value of 1.7, so Eq. (2) reduces to:

$$H = 1.7 * u_2 T_2 \tag{3}$$

Analogue to the sensible heat flux, the latent heat flux can be written as:

$$LE = \frac{\rho l_v k^2 (u_2)(q_2 - q_0)}{\ln\left(\frac{z+z_0}{z_0}\right)\ln\left(\frac{z+r_0}{r_0}\right)} \tag{4}$$

where l_v is the latent heat of vaporisation and q the specific humidity. Here an exchange coeficient of 4315 is adopted, so Eq. (4) reduces to:

$$LE = 4315 u_2 (q_2 - q_0) \tag{5}$$

The uncertainty in z_o and r_o is estimated to result in a relative error of 25% for H and LE. Using measurements at 6 m and 0.5 m to calculate the turbulent heat flux results in a contribution of only roughly 25 W/m^2 as a mean for the entire period (Duynkerke et al., 1994). Applying Eq. (3) and Eq. (5) results in turbulent heat flux of 43 W/m^2 as a mean over the entire period. The advantage of using measurements at two heights is that no roughness lengths have to be specified. The disadvantage is the larger sensitivity to instrumental errors. A comparison with detailed turbulent flux measurements should be made in order to solve the choice of the most appropriate method to calculate turbulent fluxes

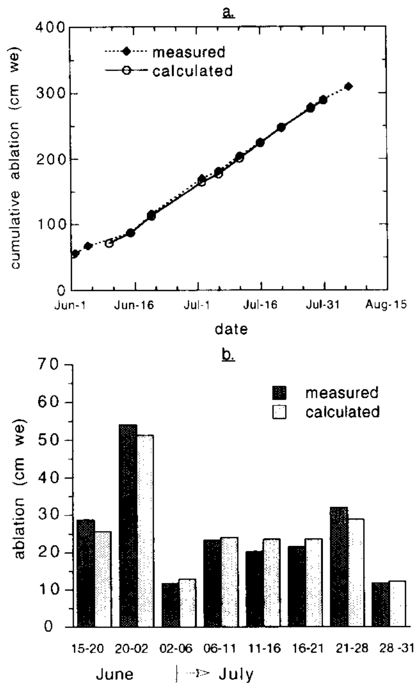

Fig. 6. (a) The measured and calculated ablation as a function of time. (b) The measured and calculated ablation in different time periods.

from simple meteorological measurements. In this paper we follow the approach defined by the Eqs. (2) to (5).

The mean values of the fluxes (W/m^2) are presented in Eq. (6):

$$\begin{aligned} B &= G(1-\alpha) + L_n + H + LE \\ 162 &= 117 + 2 + 40 + 3 \end{aligned} \qquad (6)$$

The energy available for melting (162 W/m^2) corresponds with an ablation rate of 42 mmwe/day. The energy comes roughly for 3/4 from the shortwave radiation and for 1/4 from the sensible heat flux. If we compare calculated ablation with measured ablation, a close agreement is obtained as presented for the whole period, as well as for periods of approximately 7 days (Fig. 6a, b). The cumulative difference between measured and calculated ablation over the period is less than 0.5%, a fortuitous result considering the accuracy of the calculations and measurements. An attempt to correlate differences between calculated and observed ablation using different terms in the energy balance did not reveal any significant correlation. The calculated differences can either entirely be due to the measuring inaccuracy or to the uncertainties in the calculations. It can therefore be concluded that the energy balance approach, as applied here, is valid for this period and region. The resulting curve can therefore be used to force a simple runoff model.

3. The runoff model

3.1. Description of the runoff model

For simplicity it is assumed that all input of water to the proglacial river system is of supraglacial origin as calculated in the previous section. Temporary storage of water in the glacier system and meltwater supplied by basal melting are neglected. Although this model was applied to a arid area, precipitation was included as an input parameter. The crucial point in the model is, in this particular case, the definition of the catchment area. As a start we considered a transect perpendicular to the ice margin, the transect width being defined as equidistant between the next outlet river to the north, coming from the Isunguata Sermia and the next outlet river to the south coming from the Leverett Glacier. Obviously, there may be a considerable error in such estimates, especially as one gets higher on the ice sheet (Thomsen, 1987), but a lack of bedrock data prevented a more detailed approach. The estimated values are presented in Table 2. Total discharge derived from the hydrograph between 10/7–14/8 1990 was 7.2×10^7 m^3, a quarter to

Table 2
Catchment area and the ablation as a function of altitude

Altitude (masl)	Area (km^2)	Ablation rate (mmwe/day)	Calculated ablation ($\times 10^7$ m^3)
< 350	10	45	1.2
350–450	16	43	1.9
450–750	58	40	6.5
750–1000	92–187	37	9.5–19.4
> 1000	188–400	17	8.9–19.0
Total	364–670		28 –48 Measured runoff 7.2

an eight of the areally integrated ablation. Even if we consider that the supra glacial contribution above 1000 masl is unlikely to drain to the gauged site, spatially integrated ablation is still grossly overestimated. The ablation calculated for the area under 750 masl is 9.6×10^7 m^3, providing closer agreement with measured runoff. As the gauged river is marginal to a major outlet glacier, it is unlikely that it receives meltwater travelling from the higher levels. This is confirmed by the short response time of the discharge of about eight hours. It is likely that the Isunguata Sermia and the Leverett Glacier (Fig. 1) act as major drainage routeways for the long travelled water above approximately 1000 masl. This simple bulk runoff estimate justifies the use of a local catchment area below 1000 masl from which a part drains to the southern and northern rivers. Input from the non glacierized part can be neglected because of the aridity of the area (Hasholt et al., 1978).

The model divides the glacier into two different boxes (Figure 7). The lower box corresponds to the areas at the same elevation as mast 4 and 5. The second box represents the area at the same elevation as the relay station and mast 6.

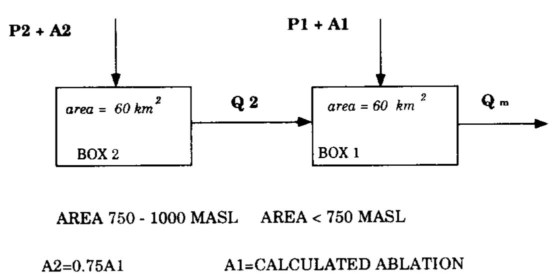

Fig. 7. A schematic picture of the runoff model. P is precipitation, A ablation, Q discharge.

Each box has an input consisting of meltwater (A) and precipitation (P) and discharge (Q_{mod}) as output. The boxes are linked to each other as shown in Fig. 7. Discharge (Q_{mod}) is defined by the following equation:

$$Q^2_{\mathrm{mod}\,i}(t) = V_i(t)C_i \tag{7}$$

where V is the volume of water stored in a box and C a constant determining the drainage velocity of the system. The subscript i represents the box number 1 or 2. Eq. (7) is a rather arbitrary chosen relation reflecting the idea that the discharge rises less than proportional with the volume of water in a box. The change of the volume of water stored in time is given by the difference in input, $A+P$ and output Q_{mod}:

$$Q_{\mathrm{mod1}}(t) = \frac{\mathrm{d}V_1}{\mathrm{d}t} - A_1(t) - P(t) + Q_{\mathrm{mod2}}(t)$$

$$Q_{\mathrm{mod2}}(t) = \frac{\mathrm{d}V_2}{\mathrm{d}t} - A_2(t) - P(t) \tag{8}$$

The ablation in the second box is proportional to the ablation in the first box as described by the regression equation for the yearly ablation (Fig. 4) and the mean elevation of the boxes, respectively 500 masl and 875 masl. This results in a ratio of 0.75 between the ablation in the second and the first box. The volume of the ablation in the boxes is the product of calculated ablation and area. Precipitation is the second, time-dependent input parameter, assumed to be equal for both boxes. The precipitation record is plotted in Fig. 8. A distinction is made between convective and non convective rain, to which we will return later.

Eqs. (7) and (8) can be solved, once the initial conditions are specified. At $t=0$ the discharge

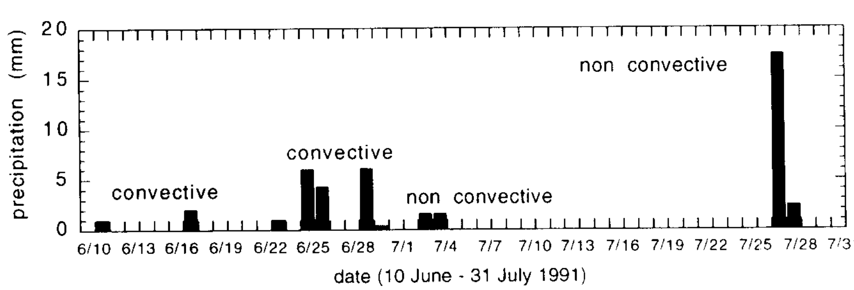

Fig. 8. The precipitation record during the measuring period.

Q_{mod1} is estimated to be equal to the mean measured discharge. The results do not depend on this initial value because the calculated ablation record is available already 12 days before the runoff record started, resulting in an adjustment of the discharge to the forcing function. Tuning parameters in the model are the area of the two boxes and the constant C.

To test a model run with an appropriate set of parameters, two performance indicators are defined. First of all we compare the mean measured discharge (Q_{meas}) with the mean modelled discharge (Q_{mod}). The mean values are determined by the area of the boxes. Adoption of a value of 60 km^2 for the first box and a value of 60 km^2 for the second box give good results, with a difference between Q_{meas} and Q_{mod} smaller than 1%. As expected these areas are less than those mentioned in Table 2 as not all the water drains to the gauged site. Another set of values summing up to approximately 120 km^2 might give the same result but will never reveal a better result regarding the second performance indicator. This indicator is defined as the mean squared error (MSE) between modelled and measured discharge during the overlapping period of the meteorological observations and the discharge measurements, June 22–July 31, 1991. The best result, displayed in Fig. 9, gives a MSE of 6.5 m^3/s equalling 13% of the mean discharge. Fig. 9 shows the forcing of

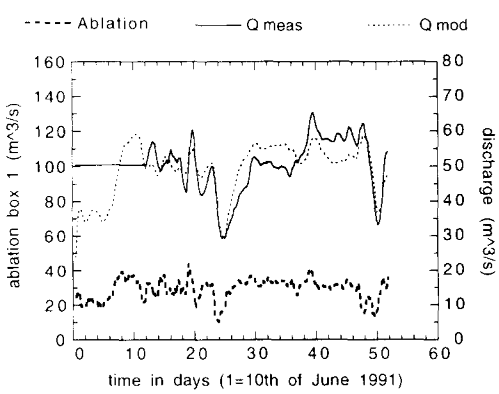

Fig. 9. The measured and modelled discharge as a function of time, together with the forcing function for box 1 (ablation). The peak in the discharge around day 48 is due to the non-convective precipitation as indicated in Fig. 8. Values are daily running mean values.

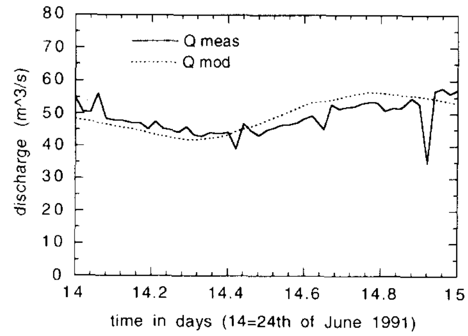

Fig. 10. A close up of the measured and modelled discharge during a day with a moderate daily cycle in the discharge.

the model (only A) as well as Q_{meas} and Q_{mod}. Obviously the model predicts correctly major drops in the discharge, for instance around July 4 and July 27. However, the increase in base flow as measured during the second half of July is not simulated, a consequence of the constant ablation rate in July, Fig. 9. But major errors in the forcing can be excluded since we showed that there is a good agreement between measured and calculated ablation. Therefore a change in catchment area or another input source should be considered for this period. The MSE is, of course, considerably influenced by the change of measured discharge to a higher level during the second part of July.

Another remarkable discharge peak around the July 28 can be explained by considerable precipitation on the day before (Fig. 8). In fact only this precipitation event contributes to a lowering of the MSE of Q_{meas} and Q_{mod}. Convective precipitation does not extend significantly over the ice sheet, being bounded to its source area, the tundra.

It can be seen for example in Fig. 10 that short time scale variations in the discharge measurements were observed regularly throughout the melt season. Filtering of these events from river discharge record reduced the MSE between the modelled and observed discharge by 2%, seeming reasonable because these events are probably solely due to ice front collapses rather than ablation rate variations. These mini flood events are described in a separate paper (Russell et al., in prep.).

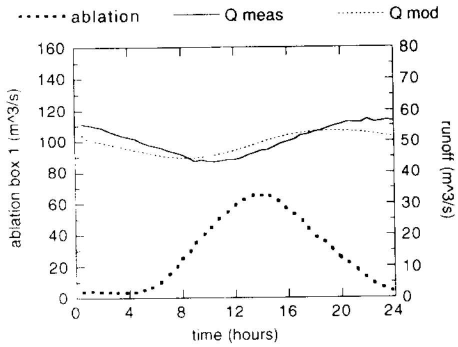

Fig. 11. Mean diurnal cycle for the measured and modelled discharge and for the ablation in box 1. The modelled discharge peaks somewhat too early and the amplitude is smaller than observed.

A shortcoming of the model is the poor agreement between Q_{meas} and Q_{mod} characterising the time delay between the maximum in the modelled and the measured discharge as displayed in Fig. 10 for a typical fine weather day, and for the mean diurnal cycle in Fig. 11. Although it is beyond the scope of this paper it can be proved that the time delay in the model is maximised to 1/4 of the forcing cycle. So in this case the maximum modelled time delay would be 6 hours whereas the measurements indicate a time delay of 8.5 hours. Fig. 11 shows a maximum for the modelled discharge at around 19 h and for the ablation around 13 h resulting in a time lag of 6 hours. Including a diffusion term in the model would probably improve the modelling of the time delay. A second shortcoming, connected to the first is the simulation of the amplitude of the diurnal cycle. Small values of the constant C lead to an amplitude far larger than measured and a response time being negligible. The adopted value for C on the other hand gives the smallest MSE, a reasonable time delay (6 hours), but an underestimate of the diurnal cycle. Large uncertainties in the catchment area and the potential error caused by the englacial water drainage half July do not justify further refinement of this model.

In spite of the shortcomings of the model, calculated and modelled discharge are in reasonable agreement as can be seen in Fig. 12a. A similar result is obtained when half hourly values of calculated and modelled discharge are correlated. Fig. 12b shows the mean daily measured runoff as a function of the calculated ablation, yielding no significant correlation for a time lag of 8.5 hours (or any other).

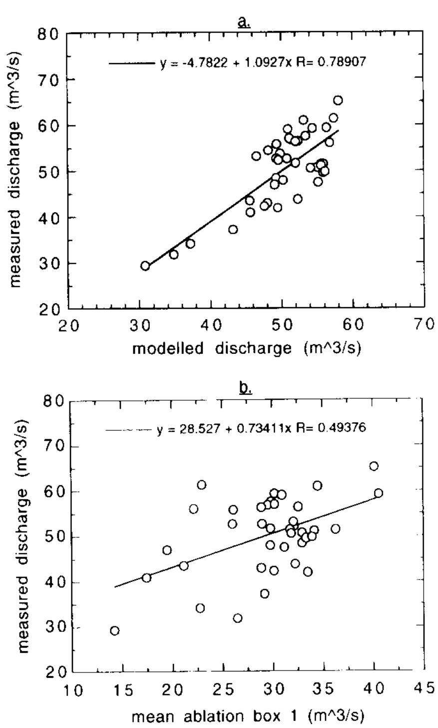

Fig. 12. (a) Scatter plot for daily mean values of modelled and measured discharge showing a significant linear correlation. (b) Scatter plot for daily mean values of calculated ablation and measured discharge showing a poor correlation. Daily mean values are calculated using a time lag of 8.5 hours as suggested by Fig. 11.

4. Concluding remarks

4.1. Energy balance model

In spite of the uncertainties in the measurements of the longwave radiation and the calculation of the turbulent heat fluxes, there was an excellent agreement between measured and calculated ablation. This does not mean that the problem of calculating ablation from meteorological measurements is solved. Errors could have been reduced by coincidence, but the most probable reasons for the success of the experiment are the conditions of low accumulation and high air temperature justifying the zero degree ice temperature assumption. Problems of extending this approach to other parts of the Greenland Ice Sheet are introduced by processes as refreezing and variations in surface temperature. This study, however, provides justification for future attempts using energy balance calculations, to model the ablation over the whole ice sheet.

4.2. Runoff modelling

Detailed modelling of the meltwater runoff from the Greenland Ice Sheet is a complicated procedure. Several factors lead to large uncertainties, for instance catchment area size and the englacial drainage and storage. Other local non meteorological factors like ice front collapsing and the development of the internal drainage system influence the proglacial meltwater runoff as well. Nevertheless reasonable results can be achieved by a bulk runoff approach with a linear box model as used in this study, to predict half hourly and daily variations adequately. More detailed modelling of runoff in this area is difficult to achieve without further glacio-hydrological data. The lack of data limits further refinement of the runoff model. To be able to predict an accurate discharge record it is necessary to have a better estimate of the drainage area. Nevertheless relatively simple measurements of water level in a proglacial river allow both daily and annual ablation variations to be monitored.

5. Acknowledgements

This work could never have been performed without the assistance of the members of the two GIMEX expeditions:, R. Bintanja, M. Portanger, W. Boot, M. van den Broeke, P.G. Duynkerke, H. Snellen, L.C. Conrads, J. Oerlemans, J.P.F. Fortuin, J. de Weger, E. Oosterbaan, F. van Tatenhove, J. Schoorl, J.J. van der Meer, and H. Jiskoot. We are also very grateful for all the support we got from the local people, especially from the staff of the Danish Meteorological Institute in Søndre Strømfjord, and from the Department of Earth Sciences of the Free University of Amsterdam for providing the pressure transducer.

Financial support for this work was obtained from the Dutch National Research Programme on Global Air Pollution and Climate Change (contract 276/91-NOP), from the Commission of the European Communities (contract EPOC-CT90-0015), and from the Netherlands Organisation for Scientific Research (Werkgemeenschap CO_2-Problematiek).

6. References

Baker, D., Escher-Vetter, H., Moser, H., Oerter, H. and Reinwarth, O., 1982. A glacier discharge model based on results from field studies of energy balance, water storage and flow. IAHS Publ., 138: 103–112.

Braithwaite, R.J., 1983. Detection of climate signal by interstake correlations of annual ablation data Qamanârssûp Sermia, West Greenland. J. Glaciol., 35 (120): 253–259.

Duynkerke, P.G. and Van den Broeke, M., 1994. Surface energy balance and atmospheric boundary layer structure near the boundary line between glacier and tundra during GIMEX 91. Global Planet. Change, 9: 17–28.

Hasholt, B. and Søgaard, H., 1978. Et forsøg på en klimatisk-hydrologisk regionsinddeling af Holsteinsborg kommune (Sisimut). Geogr. Tidsskr., 77: 72–92.

Herschy, R.W. (Editor), 1978. Hydrometry, Principles and Practices. Wiley, New York, 511 pp.

Hogg, I.G.G., Paren, J.G. and Timmis, R.J., 1982. Summer heat and ice balances on Hodges Glacier, South Georgia, Falkland Islands Dependencies. J. Glaciol., 28 (99): 221–238.

Ohmura, A. and Reeh, N., 1991. New precipitation and accumulation maps for Greenland. J. Glaciol., 37 (125): 125–148.

Russell, A.J., Van Tatenhove, F. and Van de Wal, R.S.W., in prep. The effects of ice-front collapse and flood generation on a proglacial river channel near Søndre Strømfjord, West Greenland.

Thomsen, H.H., 1987. Continued glaciological work north-east of Jakobshavn, West Greenland. Grønlands Geol. Unders. Rep., 135: 84–87.

Van den Broeke, M., Duynkerke, P.G. and Oerlemans, J., 1994. The observed katabatic flow at the edge of the Greenland Ice Sheet during GIMEX 91. Global Planet. Change, 9: 3–15.

Weidick, A., 1984. Studies of glacier behaviour and glacier mass balance in Greenland—a review. Geogr. Ann., 66A (3): 183–195.